AIP Applied Physics Letters

Measurement of probability distributions for internal stresses in dislocated crystals

Angus J. Wilkinson, Edmund Tarleton, Arantxa Vilalta-Clemente, Jun Jiang, T. Benjamin Britton, and David M. Collins

Citation: Applied Physics Letters **105**, 181907 (2014); doi: 10.1063/1.4901219
View online: http://dx.doi.org/10.1063/1.4901219
View Table of Contents: http://scitation.aip.org/content/aip/journal/apl/105/18?ver=pdfcov
Published by the AIP Publishing

Articles you may be interested in

Neutron diffraction measurements of dislocation density in copper crystals deformed at high strain rate
AIP Conf. Proc. **1512**, 526 (2013); 10.1063/1.4791143

In situ laser-based resonant ultrasound measurements of microstructure mediated mechanical property evolution
J. Appl. Phys. **107**, 063510 (2010); 10.1063/1.3327428

Microstructure and mechanical property characterizations of metal foil after microscale laser dynamic forming
J. Appl. Phys. **101**, 063108 (2007); 10.1063/1.2710334

Stress evolution during and after sputter deposition of Cu thin films onto Si (100) substrates under various sputtering pressures
J. Appl. Phys. **97**, 054908 (2005); 10.1063/1.1858062

The effects of misfit dislocation distribution and capping layer on excess stress
Appl. Phys. Lett. **74**, 1230 (1999); 10.1063/1.123508

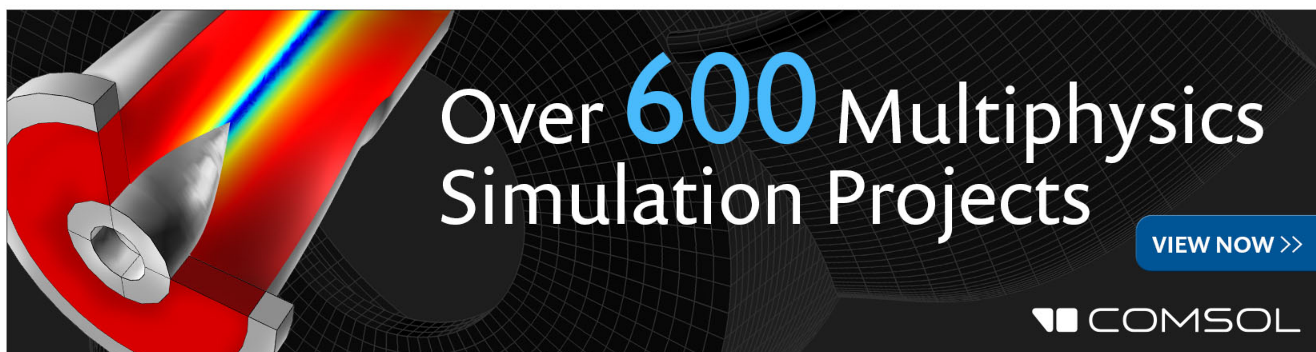

This article is copyrighted as indicated in the article. Reuse of AIP content is subject to the terms at: http://scitation.aip.org/termsconditions. Downloaded to IP: 155.198.98.141 On: Fri, 12 Dec 2014 13:35:54

APPLIED PHYSICS LETTERS **105**, 181907 (2014)

Measurement of probability distributions for internal stresses in dislocated crystals

Angus J. Wilkinson,[1] Edmund Tarleton,[1] Arantxa Vilalta-Clemente,[1] Jun Jiang,[2] T. Benjamin Britton,[2] and David M. Collins[1]
[1]*Department of Materials, University of Oxford, Parks Road, Oxford OX1 3PH, United Kingdom*
[2]*Department of Materials, Imperial College London, Royal School of Mines, Exhibition Road, London SW7 2AZ, United Kingdom*

(Received 6 August 2014; accepted 27 October 2014; published online 7 November 2014)

Here, we analyse residual stress distributions obtained from various crystal systems using high resolution electron backscatter diffraction (EBSD) measurements. Histograms showing stress probability distributions exhibit tails extending to very high stress levels. We demonstrate that these extreme stress values are consistent with the functional form that should be expected for dislocated crystals. Analysis initially developed by Groma and co-workers for X-ray line profile analysis and based on the so-called "restricted second moment of the probability distribution" can be used to estimate the total dislocation density. The generality of the results are illustrated by application to three quite different systems, namely, face centred cubic Cu deformed in uniaxial tension, a body centred cubic steel deformed to larger strain by cold rolling, and hexagonal InAlN layers grown on misfitting sapphire and silicon carbide substrates. © *2014 AIP Publishing LLC*.
[http://dx.doi.org/10.1063/1.4901219]

Electron backscatter diffraction (EBSD) is a scanning electron microscope based technique in which the scattering of low-energy-loss electrons as they exit through the top few tens of nanometers leads to Kikuchi diffraction.[1–4] Analysis for determining elastic strain variations has been established using cross-correlation measurements of small shifts in pattern features relative to their positions in a reference pattern.[5,6] Iterative schemes employing multiple passes of cross-correlation combined with remapping of the test pattern intensities have been developed[7,8] to enable reliable recovery of elastic strains in the presence of larger effects from lattice rotations that dominate in deformed metals.[9–11] Despite this, the stresses measured using EBSD are sometimes rather higher than some researchers' expecttions. In this letter, we demonstrate that these stress values are physically reasonable and are an inevitable result of the high spatial resolution of the stress measurement coupled with the presence of dislocations in the sample, which generate very high but localised stresses.

Measurements were made on the following sample sets: (i) Czochralski silicon was used as a dislocation free control sample, (ii) polycrystalline copper (face centre cubic) deformed to tensile strains of 0%, 2%, 6%, and 10%,[11,12] (iii) DX54 ferritic steel (body centred cubic) plates in an annealed state and after cold rolling to 33% and 50% thickness reductions, and (iv) two InAlN/AlN/GaN High Electron Mobility Transistor (HEMT) structures (hexagonal) grown by Metal Organic Vapour Phase Epitaxy (MOVPE) on 4H-SiC and sapphire substrates.[13]

EBSD patterns were recorded using a JEOL 6500F FEG-SEM equipped with a TSL Digiview II EBSD system (∼1000 × 1000 pixel CCD device). Patterns were recorded over square grids with step sizes of 500 nm for the Cu and Si control sample, 600 nm for the steel, and 100 nm for the InAlN samples. The patterns were recorded to hard disk with maps varying in size from ∼51 k points for the Cu samples to ∼110 k points for the steel. Cross-correlation based analysis for elastic strain and therefore stress were undertaken off-line using methods described in Refs. 5–7 and 9 with two iterations with an intermediate pattern remapping used for the Cu and steel but only a single iteration of cross-correlation used for the InAlN and Si samples. Automated procedures for selecting reference points within each grain were used,[12] and the average elastic strains and stresses were set to zero within each grain.[11]

Each EBSD dataset consisted of a map showing the spatial distribution of the stress tensor variation from the average within each grain (i.e., stress fluctuations of type III according to Masing's classification[14,15]). Histograms were constructed for each dataset showing the probability $P(\sigma_{ij})$ of finding a given stress level within the map as simply the number of

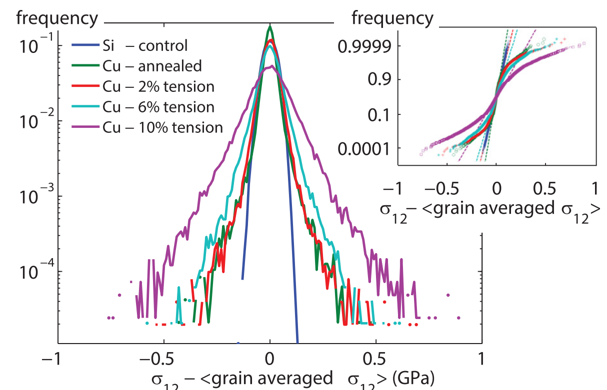

FIG. 1. Stress σ_{12} probability distributions measured by EBSD in Cu polycrystals deformed to 4 different plastic strain levels and a control Si sample. Note the use of a log-scale for the probability axis in the main plot so as to emphasise the low probability tails. Inset are normal probability plots where the straight line for the Si control data indicates that it is well represented by a Gaussian distribution.

 © 2014 AIP Publishing LLC

This article is copyrighted as indicated in the article. Reuse of AIP content is subject to the terms at: http://scitation.aip.org/termsconditions. Downloaded to IP: 155.198.98.141 On: Fri, 12 Dec 2014 13:35:54

points at a given stress level divided by the total number of data points (examples shown in Figure 1(a) for Si and Cu samples). A log-scale is used for probability to emphasise the differences between the datasets which are most obvious in the tails. The central parts of these distributions are well represented by Gaussian functions as demonstrated by the linear response when these data are plotted on a normal probability plot such as Figure 1(inset). For the control Si sample, the whole distribution fits well to a Gaussian and the gradient of the normal probability plot corresponds to a standard deviation of 32 MPa. However, significant contributions to this come from errors in correcting for pattern shifts induced by displacement of the electron beam across the sample.[5] Small misalignments in mounting the sample lead to errors in the sample geometry and hence the calculated beam displacement across the sample which is evident as near linear stress variations across the maps. The map on the Si sample covers an area of 150 μm $\times$ 150 μm which is considerably larger than the typical grain size in the other maps. Restricting the analysis to a 30 μm $\times$ 30 μm section more representative of a grain area reduces the standard deviation to 22 MPa, which corresponds to a strain error of $\sim 2.8 \times 10^{-4}$ which is in reasonable agreement with the previous estimates.[5,16]

For the Cu data, the central part of the distribution is well represented by a Gaussian. At high stress magnitudes, the probabilities above that expected are referred to as "tails". In these plots, the extent of the tails is exaggerated due to the log-scale, though these high stress regions correspond to small fraction of the data. The departure from Gaussian-like probability distributions moves to lower stress magnitudes as the plastic deformation level increases. Attributing these high stress values to dislocations within the crystals agrees well with both the absence of tails for the dislocation-free Si and the increasing strength of the tails as dislocation density increases with deformation in the Cu.

Analysis of the stress field, σ_{ij}, near a dislocation provides a more quantitative test to determine whether these probability distributions are due to isolated dislocations. Groma and co-workers have given a mathematically rigorous analysis of the asymptotic behaviour of the probability distribution at high stresses for systems containing many parallel straight dislocations,[17,18] and shown how this can be used in analysis of X-ray peak broadening.[19] The similarity between broadening of X-ray peak profiles and stress probability distributions generated by dislocations was also noted by Zaiser and Seeger.[20] The multiple overlap of fields from each dislocation makes the analysis mathematically demanding, however, using the conceit that the system can be split into a series of patches within which the stress is dominated by the field from the one nearest dislocation allows a simple analysis which captures the main result. Figure 2 shows one such patch of area A_0 in which the stresses will of course be largest near the centre as this is close to the dislocation.

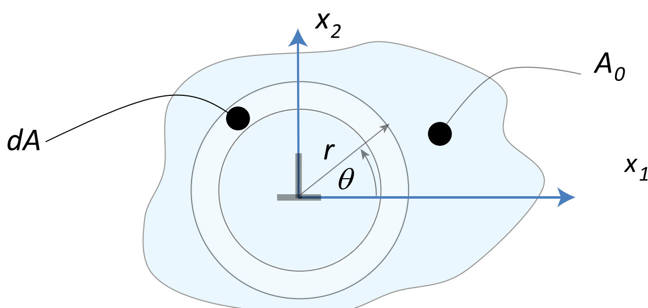

FIG. 2. Schematic diagram illustrating a patch of material area A_0 in which stress is dominated by the edge dislocation towards the patch centre.

The stress near a single edge dislocation can be written

$$\sigma_{ij} = \frac{D\,K_{ij}(\theta)}{r} \tag{1}$$

for a dislocation line along the x_3 axis with Burgers vector magnitude b along the x_1 axis from which the angle θ is measured and r is the radial distance from the dislocation. The constant D is given in terms of the shear modulus G and Poisson ratio ν by

$$D = \frac{G\,b}{2\pi(1-\nu)}, \tag{2}$$

while K_{ij} gives the angular dependence of the stress which differs for each stress component. For the shear stress σ_{12}, K_{12} is given by

$$K_{12} = \cos(\theta)\cos(2\theta). \tag{3}$$

Inspection of Figure 2 shows that in the limit of high stresses near an isolated dislocation the probability can be established from the fractional area of the patch

$$P = \frac{\mathrm{d}A}{A_0} = \frac{r\mathrm{d}\theta\,\mathrm{d}r}{A_0}. \tag{4}$$

Combining (1) and (4) leads to

$$P(\sigma,\theta) = \frac{D^2K^2(\theta)\,\mathrm{d}\theta}{A_0}\frac{\mathrm{d}\sigma}{\sigma^3}. \tag{5}$$

Integrating around an annulus radius r with width dr allows the angular variation to be averaged, giving the probability as a function of stress

$$P(\sigma) = \frac{D^2\langle K^2\rangle}{A_0}\frac{\mathrm{d}\sigma}{\sigma^3}, \tag{6}$$

where

$$\langle K^2\rangle = \int_0^{2\pi} K^2(\theta)\,d\theta \;\rightarrow\; \langle K_{12}^2\rangle = \pi/2. \tag{7}$$

Equation (6) shows that the high stress tails of the probability distributions should be proportional to σ^{-3}. As there is one dislocation within the patch the dislocation density (ρ_0) is given by $1/A_0$ and so the strength of the tail is proportional to the dislocation density. As the tails correspond to low probability, where experimental data tends to be somewhat noisy, rather than fitting the data directly to Eq. (6), we follow Groma[19] and use the restricted second moment v_2 of the probability

This article is copyrighted as indicated in the article. Reuse of AIP content is subject to the terms at: http://scitation.aip.org/termsconditions. Downloaded to IP: 155.198.98.141 On: Fri, 12 Dec 2014 13:35:54

$$v_2(\sigma) = \int_{-\sigma}^{+\sigma} P(\sigma)\,\sigma^2\,d\sigma \;\rightarrow\; \frac{D^2\langle K^2\rangle}{A_0}\ln(\sigma) = D^2\langle K^2\rangle\rho_0\ln\left(\frac{\sigma}{\sigma'}\right) = \frac{(Gb)^2}{8\pi(1-\nu)^2}\rho_0\ln(\sigma/\sigma'). \tag{8}$$

A plot of the restricted second moment against $\ln(\sigma_{ij})$ should tend to a straight line at high stress if the probability distribution is proportional to σ^{-3} and the integral form reduces the noise level compared to fitting the σ^{-3} distribution directly.

To validate this approach, two dimensional discrete dislocation dynamics simulations were used. A set of N edge dislocations were randomly positioned in a square cell of side length L. All dislocations had their line direction parallel to the x_3 axis out of the plane of the cell and half had a Burgers vector along the positive x_1 axis and half along the negative x_1 axis. A dislocation dynamics simulation was used to relax the dislocation structure, with periodic boundary conditions imposed. Dislocation velocities were taken to be linearly proportional to the shear stress acting at the dislocation position and a variable time step was used to evolve the dislocation positions. Dislocation pairs were removed whenever positive and negative dislocations came within $5b$. The simulations allowed the analysis above to be assessed using stresses sampled from simulation cells containing known densities of dislocations.

Figure 3(a) shows a field plot of the shear stress for one such simulation with cell size $L = 10\,\mu$m after relaxation during which the initial 10 000 randomly positioned dislocations reduced to a final content of 5730. The stresses were sampled on a grid of 800 × 800 points (i.e., 640 k points) to construct the map, illustrating the extreme high and low values resulting from near coincidence of the grid point and a dislocation position. After relaxation, the stress probability distribution for these simulations was broadly similar to those found experimentally. Figure 3(b) shows a central low stress magnitude region following a Gaussian distribution with pronounced tails at the high magnitude stresses. A plot of the restricted second moment v_2 against $\log(\sigma_{12})$ suggested by Eq. (8) is shown in Figure 3(c) for the simulation depicted in Figures 3(a) and 3(b). The curve tends to a straight line at higher stresses and using the gradient obtained from a straight line fit to the portion of the curve marked in red allows the dislocation density to be determined. This procedure was repeated for various simulations at different dislocation densities and stress sampling point spacings. The inset in Figure 3(c) shows that the gradient of the v_2 against $\ln(\sigma_{12})$ allows the total dislocation density to be recovered with good accuracy especially when there are a large number of stress measurements available.

Figure 4(a) shows similarly the v_2 against $\ln(\sigma_{12})$ plots for the experimental HR-EBSD measurements obtained from the Cu samples at four different deformation states. The data all exhibit the expected linear relationship at higher stress values. The gradients of these plots systematically increase with plastic strain level for the Cu samples which is expected due to the increasing dislocation density with strain. The dislocation densities obtained for the four Cu samples are given in Table I and are compared to geometrically necessary dislocation (GND) densities obtained using a Nye tensor-based analysis and the EBSD measured lattice curvatures.[10,12] For some cases, the total dislocation density assessed through equation 8 is smaller than the GND density which should be only a fraction of the total density. This is

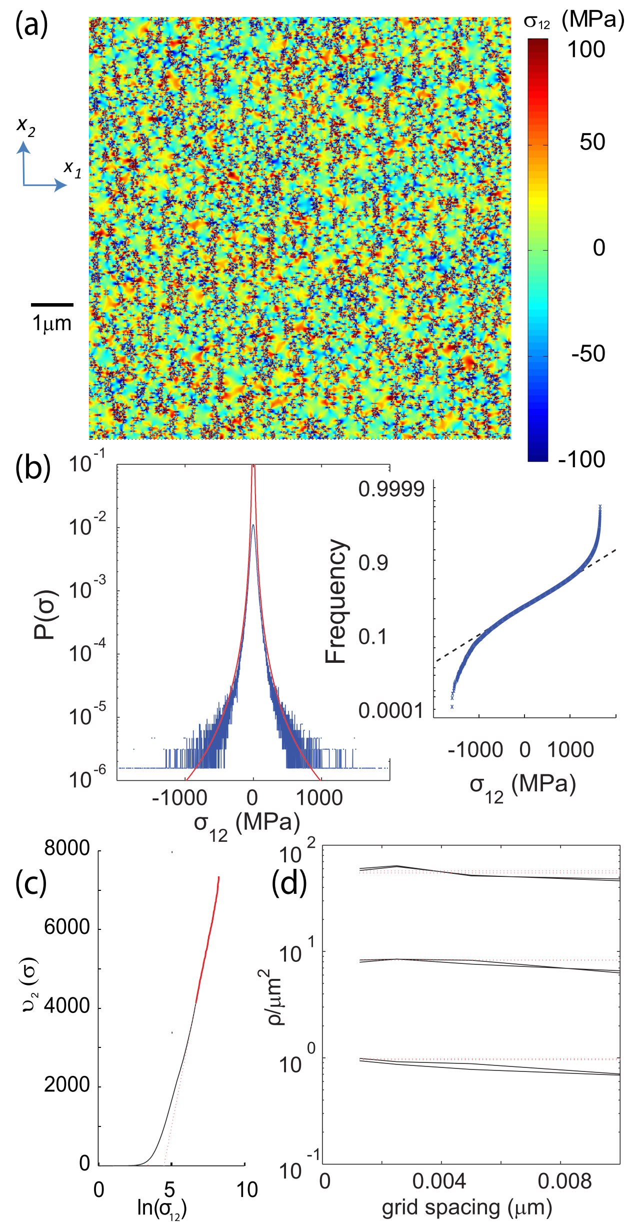

FIG. 3. Discrete dislocation dynamics simulation results. (a) Shear stress field (sampled on a 800 × 800 grid) from the relaxed dislocation structure with a final total dislocation density of 5.73×10^{13} m^{-2}. (b) Frequency vs stress distribution, (c) restricted second moment of stress probabilty distribution versus logarithim of stress showing linear varition at high stress (red section). (d) Convergence of dislocation density recovered from gradient of restricted second moment plots as a function of grid spacing for stress sampling. Dotted lines indicate known dislocation densities in $10\,\mu$m square cell.

TABLE I. Dislocation densities obtained for four Cu samples.

Deformation state	Annealed	2%	6%	10%
GND density ($\times 10^{12}$ m^{-2})	27	100	121	257
Total density ($\times 10^{12}$ m^{-2})	39	54	122	445

This article is copyrighted as indicated in the article. Reuse of AIP content is subject to the terms at: http://scitation.aip.org/termsconditions. Downloaded to IP: 155.198.98.141 On: Fri, 12 Dec 2014 13:35:54

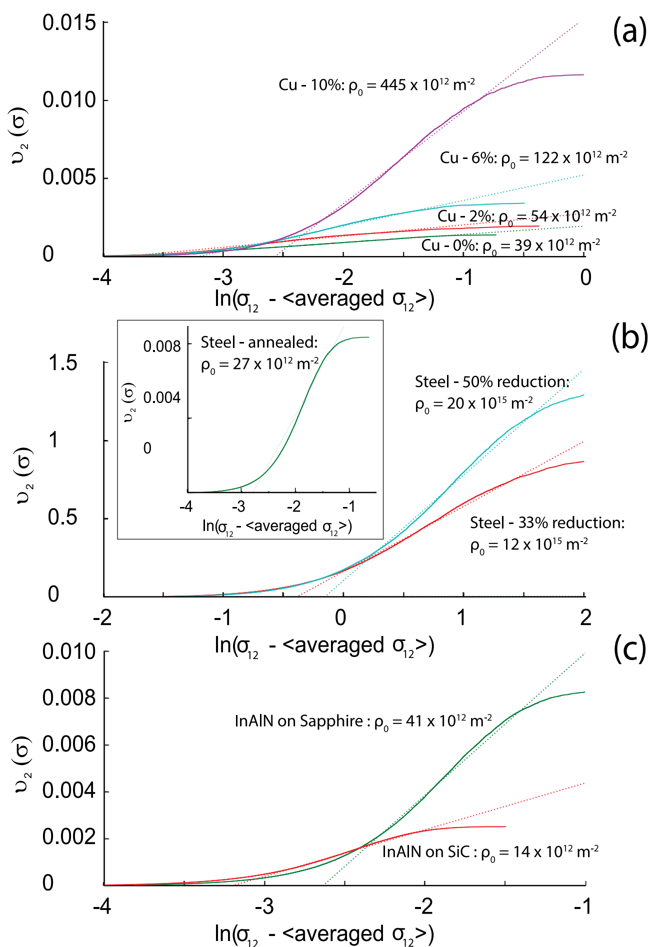

FIG. 4. Plots of the restricted second moment v_2 against $\ln(\sigma_{12})$ suggested by Eq. (8) for (a) the Cu samples in the annealed condition and after plastic strain to 2%, 6%, and 10%, (b) for ferritic steel samples in the annealed condition and after rolling reductions of 33% and 50%, and (c) for two InAlN samples one grown on a sapphire substrate and the other on SiC.

likely due to the simplified geometry of a single set of edge dislocations used to establish the pre-factor in Eq. (8). In reality, multiple dislocations types with differing line directions and Burgers vectors will be present. Since the σ_{12} stresses tend to become smaller as the Burgers vector is moved out of the x_1–x_2 plane the pre-factor in Eq. (8) will tend to underestimate the total dislocation density.

The analysis was extended to higher plastic strains and BCC crystallography by investigating ferritic steel sheet samples before and after cold rolling to 33% and 50% thickness reduction. Figure 4(b) shows the restricted second moment plot for EBSD stress measurements made on these steel samples. As before, the data show a straight line variation at the higher stress levels. For the annealed sample, the low gradient indicates a low dislocation density (2.7×10^{13} m^{-2}) which is reasonable for annealed low carbon steel. The dislocation density is much higher after the considerable strain imparted by cold rolling and reaches 12×10^{15} m^{-2} at 33% reduction and 20×10^{15} m^{-2} after 50% reduction. High dislocation densities of the same order been reported; for example, a dislocation density of $\sim 10 \times 10^{15}$ m^{-2} has been estimated from an 80% reduction of a ferrite/martensite 0.2%C steel.[21]

Finally, samples of InAlN/AlN/GaN HEMT heterotructures grown on sapphire and SiC were used to investigate lower dislocation density cases. Here, the dislocations are either inherited from the substrate as the epitaxial layer is grown or generated through the lattice and thermal mismatch between the nitride layers and the substrates. The v_2 against $\ln(\sigma_{12})$ plots for these samples are shown in Figure 4(c) and are linear for the higher stress values. The gradients reveal dislocation densities of 41×10^{12} m^{-2} (4.1×10^9 cm^{-2}) for the sapphire substrate and considerably smaller for the SiC at 14×10^{12} m^{-2} (1.4×10^9 cm^{-2}). The In content was slightly different for the two samples (17.6% on the sapphire compared to 21.4% on the SiC). The Burgers vector and elastic constants used in the analysis were altered slightly according to the corrected Vegard's law to account for changes in lattice parameters and elastic constants given by Darakchieva *et al.*[22] Electron channelling contrast imaging observations on these samples have previously reported dislocation densities of 2.4×10^9 cm^{-2} and 1.4×10^9 cm^{-2} for the films on sapphire and SiC, respectively.[13] Of these, only a small fraction ($\sim$10% for sapphire, $\sim$1% for SiC) were observed to be screw $\langle \mathbf{c} \rangle$ type which would not contribute to the σ_{12} shear stress analysed here while the remaining edge $\langle \mathbf{a} \rangle$ type and mixed $\langle \mathbf{c+a} \rangle$ type dislocations contribute equally to σ_{12}. The level of agreement between these direct observations and the density implied from the statistics of the extreme stress values is good.

It seems clear from the analysis and data we have presented above that the large stress values observed in EBSD maps occur when the electron probe happens to be placed very close to the position of a near surface dislocation within the sample. The probability distributions found in a range of different sample types all exhibit the σ^{-3} variation expected from analysis of stresses near isolated dislocation. The strength of the σ^{-3} tails also increases with deformation level as would be expected and is absent in the control Si sample which does not contain dislocations. The σ^{-3} tails provide an opportunity to quantify the total dislocation density within the sample and we have made a first attempt to do that here through Eq. (8). The analysis presented here involves only a single dislocation type and extending this to multiple dislocation types including those inclined to the surface must be considered to improve the quantitative analysis.

This work was supported under EPSRC Grant Nos. EP/I021043/2, EP/J016098/1, and EP/K032518/1. A.J.W. acknowledges insightful discussion with Professor István Groma (Department of Materials Physic, Eötvös Loránd University, Hungary). We are grateful to Dr. Gamarra and Dr. Forte-Poisson (Alcatel-Thales, III-V Lab, France) for supplying the InAlN samples.

[1]D. Dingley, J. Microsc. Oxford **213**, 214 (2004).
[2]S. I. Wright and B. L. Adams, Metall. Trans. A **23**(3), 759 (1992).
[3]N. C. Krieger-Lassen, The Technical University of Denmark/Risø National Laboratory, 1994.
[4]A. J. Wilkinson and T. B. Britton, Mater. Today **15**(9), 366 (2012).
[5]A. J. Wilkinson, G. Meaden, and D. J. Dingley, Ultramicroscopy **106**(4–5), 307 (2006).
[6]A. J. Wilkinson, G. Meaden, and D. J. Dingley, Mater. Sci. Technol. **22**(11), 1271 (2006).
[7]T. B. Britton and A. J. Wilkinson, Ultramicroscopy **114**, 82 (2012).
[8]C. Maurice, J. H. Driver, and R. Fortunier, Ultramicroscopy **113**, 171 (2012).
[9]T. B. Britton and A. J. Wilkinson, Ultramicroscopy **111**(8), 1395 (2011).

This article is copyrighted as indicated in the article. Reuse of AIP content is subject to the terms at: http://scitation.aip.org/termsconditions. Downloaded to IP: 155.198.98.141 On: Fri, 12 Dec 2014 13:35:54

[10]P. D. Littlewood, T. B. Britton, and A. J. Wilkinson, Acta Mater. **59**(16), 6489 (2011).
[11]J. Jiang, T. B. Britton, and A. J. Wilkinson, Acta Mater. **61**(15), 5895 (2013).
[12]J. Jiang, T. B. Britton, and A. J. Wilkinson, Acta Mater. **61**(19), 7227 (2013).
[13]G. Naresh-Kumar, B. Hourahine, A. Vilalta-Clemente, P. Ruterana, P. Gamarra, C. Lacam, M. Tordjman, M. A. di Forte-Poisson, P. J. Parbrook, A. P. Day, G. England, and C. Trager-Cowan, Phys. Status Solidi A **209**(3), 424 (2012).
[14]G. Masing, "Eigenspannungen in kaltgereckten Metallen," Z. Tech. Phys. **6**, 569 (1925).
[15]P. J. Withers and H. K. D. H. Bhadeshia, Mater. Sci. Technol. **17**(4), 355 (2001).
[16]T. B. Britton, J. Jiang, R. Clough, E. Tarleton, A. I. Kirkland, and A. J. Wilkinson, Ultramicroscopy **135**, 126 (2013).
[17]I. Groma and B. Bako, Phys. Rev. B **58**(6), 2969 (1998).
[18]F. F. Csikor and I. Groma, Phys. Rev. B **70**(6), 064106 (2004).
[19]I. Groma, Phys. Rev. B **57**(13), 7535 (1998).
[20]M. Zaiser and A. Seeger, *Dislocations in Solids* (North Holland, 2002), Vol 11, p. 1.
[21]S. Takaki, S. Iizuka, K. Tomimura, and Y. Tokunaga, Mater. Trans. JIM **33**(6), 577 (1992).
[22]V. Darakchieva, M.-Y. Xie, F. Tasnádi, I. A. Abrikosov, L. Hultman, B. Monemar, J. Kamimura, and K. Kishino, Appl. Phys. Lett. **93**(26), 261908 (2008).

This article is copyrighted as indicated in the article. Reuse of AIP content is subject to the terms at: http://scitation.aip.org/termsconditions. Downloaded to IP: 155.198.98.141 On: Fri, 12 Dec 2014 13:35:54